Oxygen exchange kinetics of $La_{0.6}Sr_{0.4}CoO_{3-\delta}$ affected by changes of the surface composition due to chromium and silicon poisoning

E. Bucher* (1), C. Gspan (2), T. Höschen (3), F. Hofer (2), and W. Sitte (1)

(1) Chair of Physical Chemistry, Montanuniversitaet Leoben, Franz-Josef-Straße 18, 8700 Leoben, Austria

(2) Institute for Electron Microscopy and Nanoanalysis (FELMI), Graz University of Technology & Graz Center for Electron Microscopy (ZFE), Austrian Cooperative Research (ACR), Steyrergasse 17, 8010 Graz, Austria

(3) Max Planck Institute for Plasma Physics, Boltzmannstraße 2, 85748 Garching, Germany

Abstract

The long-term stability of the mixed-conducting perovskite oxide $La_{0.6}Sr_{0.4}CoO_{3-\delta}$ (LSC) was investigated for 3400 h at 800°C. The oxygen exchange kinetics of LSC was studied in-situ in dry and humidified atmospheres in the absence as well as the presence of Cr and Si sources. The chemical surface exchange coefficient (k_{chem}) and the chemical diffusion coefficient (D_{chem}) of oxygen were measured by the dc-conductivity relaxation method. Degraded samples were analyzed by scanning electron microscopy (SEM) with energy and wavelength dispersive X-ray spectroscopy (EDXS/WDXS), X-ray photoelectron spectroscopy (XPS), and analytical scanning transmission electron microscopy (STEM).

In dry atmosphere with 10 % O_2 high values of $k_{chem}=1\times10^{-3}$ cm s^{-1} and $D_{chem}=2\times10^{-5}$ cm^2 s^{-1} were found. A stable performance was observed during 1300 h without or with the presence of Cr- and Si-impurities. However, a significant decrease in k_{chem} and D_{chem} occurred when

the atmosphere was humidified (30-60 % relative humidity). XPS depth profiles showed Sr-enrichment and Co-depletion of the surface already during 1300 h in dry atmosphere. After the treatment in humidified atmospheres for additional 2100 h significant amounts of Cr and Si contaminations were found. SEM and STEM showed crystallites of $SrCrO_4$ and La-silicate on the surface. $SrCrO_4$ and Co_3O_4 were also found at the grain boundaries in the near-surface region. It can be concluded that the observed decrease in the oxygen exchange kinetics is closely related to significant changes of the surface composition as a result of Cr and Si poisoning which leads to the decomposition of the oxygen exchange-active LSC phase into inactive secondary phases.

Keywords: $La_{0.6}Sr_{0.4}CoO_{3-\delta}$; solid oxide fuel cell cathode; long-term stability; degradation; chromium poisoning; silicon poisoning.

*Corresponding author: Dr. Edith Bucher, Chair of Physical Chemistry, Montanuniversitaet Leoben, Franz-Josef-Straße 18, 8700 Leoben, Austria; tel.: ++43 3842 402 4813; fax: ++43 3842 402 4802; e-mail address: edith.bucher@unileoben.ac.at

1. Introduction

Solid oxide fuel cells (SOFCs) convert the chemical energy of various fuels (H_2, CH_4, diesel reformate, biogas, etc.) into electrical energy with high efficiency, producing lower emissions and less noise compared to conventional energy conversion systems based on the combustion of fossil fuels [1-3]. Although significant improvements have been reached in the SOFC technology with regard to performance and efficiency, long-term degradation remains one of the main barriers for the commercialization on a larger scale [2]. In this respect, lifetimes of SOFC systems of 5-10 kh for mobile applications and 45-100 kh for stationary applications would be required [4].

Many of the degradation phenomena which currently limit the long-term stability of SOFCs occur at the cathode surface and/or at the cathode-electrolyte interface. For example, chromium poisoning of the cathode is caused by gas phase transport of volatile Cr-species released from metallic interconnects or balance-of-plant (BOP) components and their reaction with the cathode [1, 5]. Even though protective layers for interconnects, which are applied as a thin coating or developed in-situ by high-temperature scale formation, have been developed, the complete suppression of the volatilization of Cr-species into the gas phase is not possible [1, 6, 7]. Similarly, Si poisoning of the cathode may be caused by silicon species released into the gas stream from silicate-based glass sealing materials or heat-resistant alloys used in BOP-components [8-10].

$La_{0.6}Sr_{0.4}CoO_{3-\delta}$ (LSC) is an attractive cathode material for intermediate temperature solid oxide fuel cells due to its fast oxygen exchange kinetics, high electronic and significant ionic conductivity at 600-800°C [11]. However, during long-term application, degradation of LSC occurs, especially in ambient (humid) air in the presence of Cr- and Si-impurities [12, 13]. Recent investigations at 600 and 700°C showed that the degradation is connected with the segregation of strontium from the bulk to the surface via the grain boundaries, and that these

Sr-rich interface and surface layers form inactive secondary phases (chromates, silicates, binary/ternary oxides) with the impurities [12-14].

In the present work, the long-term stability of LSC against Cr and Si poisoning in dry and humidified atmospheres is investigated during 3400 h at 800°C. The time-dependent evolution of the chemical surface exchange coefficient (k_{chem}) and the chemical diffusion coefficient of oxygen (D_{chem}) is monitored in-situ by the dc-conductivity relaxation method [15-17]. In order to gain further insight into the changes in the near-surface microstructural and compositional changes, and thus into the degradation mechanisms, post-test analyses were performed by complementary techniques: Scanning electron microscopy (SEM) with energy and wavelength dispersive X-ray spectroscopy (SEM-EDXS/WDXS) provides an overview on the microstructure and the lateral distribution of the elements and contaminants on the surface. Elemental depth profiles of the near-surface region were obtained by X-ray photoelectron spectroscopy (XPS) combined with Ar-sputtering. Analytical scanning transmission electron microscopy (STEM) with EDXS and electron energy loss spectroscopy (EELS) were used to study the chemical composition and local distribution of secondary phases at the surface and at grain boundaries with high lateral resolution.

2. Experimental details

LSC powder was provided by EMPA (Dübendorf, Switzerland). A dense cylindrical pellet was obtained by isostatic pressing at 250 MPa and sintering for 10 h at 1200°C in air with heating and cooling rates of 2 K min^{-1}. The density of the sintered sample was 98.8 % of the theoretical density. A thin platelet with a cross section of approximately 6×6 mm^2 was cut from the sintered tablet using a diamond wire saw (Well Diamond Wire Saws, Inc.). The sample was ground with a diamond grinding disk and polished with diamond lapping films

with 30, 6 and 1 µm particle size to a final thickness of 596 µm. Gold wires were attached to the four corners of the sample using gold paste (Metalor) to obtain electrical contacts.

The oxygen exchange kinetics was measured in-situ by the four-point dc-conductivity relaxation method at 800°C using the van der Pauw electrode configuration [15, 17, 18]. Oxidation and reduction steps were performed in the interval $1.0\times10^{-1} \leq pO_2/bar \leq 1.5\times10^{-1}$ in dry and humidified O_2-Ar test gases. The chemical surface exchange coefficient (k_{chem}) and the chemical diffusion coefficient (D_{chem}) of oxygen were obtained by non-linear regression of the corresponding solution of the diffusion equation [19] to the conductivity relaxation data. A pellet of pure chromium which was placed close to the sample acted as a Cr source. The quartz glass reactor served as a Si source.

Scanning electron microscopy with energy dispersive and wavelength dispersive X-ray spectroscopy (SEM-EDXS, SEM-WDXS) was performed with a Zeiss Ultra 55 microscope with an EDAX Phoenix EDXS detector and an EDAX TEX WDXS detector. Elemental distribution maps were recorded using a FEI Quanta 200 microscope with an EDAX Genesis detector for EDXS. High resolution images were acquired in secondary electron (SE) and backscattered electron (BSE) mode. Additional SEM images were recorded with a Zeiss EVO 50 SEM equipped with a LaB_6 cathode.

X-ray photoelectron spectroscopy (XPS) was performed with a Perkin Elmer PHI 5600 ESCA system with a hemispherical analyzer using Mg-Kα radiation (1253.6 eV). The analyzer was operated at constant pass energy of 58.7 eV. For depth profiling an Atomika WF 421 Microfocus Ion Gun was used. The sputter rate was estimated from the Ar^+-fluence by assuming a yield of 2 target atoms per impinging Ar^+, considering the volume density of the bulk composition [20]. A Shirley background function was applied for the background subtraction. The concentrations of the elements were obtained from the core-level peak areas using standard relative sensitivity factors.

STEM analyses were performed on a FEI Tecnai F20 (operating at 200 kV) and a FEI Titan³ G2 60-300 (operating at 300 kV), respectively. The latter is equipped with a C_S probe corrector (DCOR) for high resolution STEM imaging with a sub-Angstrom resolution, and with a high-end post-column electron energy filter (GIF Quantum ERS™) from Gatan Inc. For analytical investigations, EDXS and EELS measurements were conducted on the Tecnai F20 and the Titan³ G2. For EDXS quantification, the spectra from the Tecnai F20 were used, and for the elemental mapping the EDX and EEL spectra from the Titan³ G2 were utilised.

3. Results and Discussion

3.1 Oxygen exchange kinetics

Figures 1 (a) and 1 (b) show the kinetic parameters for oxygen exchange of LSC as a function of time at 800°C. Examples for electrical conductivity relaxation curves at different stages of the long-term stability test are given in figure 1 (c). The curves could be well described by fits of the diffusion model to the experimental data. In dry atmosphere the fresh sample exhibited high values of $k_{chem}=1\times10^{-3}$ cm s^{-1} and $D_{chem}=2\times10^{-5}$ cm^2 s^{-1}. No degradation was observed during 1300 h without or with the presence of Cr and Si sources. However, after the humidified atmosphere (30 % relative humidity) was introduced, a decrease in k_{chem} and D_{chem} was found in the presence of Cr and Si. This is due to the significant increase in the volatility of Cr gas phase species which are formed in humid atmospheres with a Cr source. The predominating compound in humid atmosphere is $CrO_2(OH)_2(g)$ which has a concentration which is by a factor of 30-70 higher than that of $CrO_3(g)$ (partial pressures estimated from thermodynamic data are given in figure 2 (for specific values see supplementary material). In addition, the humidification of the gas phase also leads to the formation of the volatile

compound $Si(OH)_4$ in the presence of a Si source, compare figure 2 (for specific values see supplementary material).

No significant increase in the degradation behavior resulted from the increase in the amount of relative humidity from 30 to 60 %, figure 1. After 3400 h k_{chem} and D_{chem} had decreased by factors of 5 and 6, respectively, resulting in final values of $k_{chem}=2\times10^{-4}$ cm s^{-1} and $D_{chem}=7\times10^{-6}$ cm^2 s^{-1}. Figure 3 shows that the electronic conductivity of the sample remained at a high level of approximately 1600 S cm^{-1} during the whole duration of the experiment (3400 h). This indicates that the degradation mainly affects the near-surface region of the sample while the bulk remains unchanged. Post-test analyses confirm that this is indeed the case (sections 3.2-3.4). In principle one would also expect D_{chem} – as a bulk parameter – to remain stable because the degradation mainly affects the surface. A possible explanation for the observed decrease in D_{chem} in the degraded sample could be the formation of secondary phases at the surface and at grain boundaries in the near-surface region (compare figures 4, 5, 7, and 8). It is possible that these regions exhibit a smaller D_{chem} for oxygen transport than the bulk phase LSC. It should be mentioned that in this case the measured parameter D_{chem} would represent an effective rate constant containing the contributions of different phases. However, a deconvolution of these effects is not possible due to the lack of data (amount, distribution, and diffusion coefficients of the secondary phases). Even though the values of D_{chem} of the degraded sample may therefore be influenced by increased measurement uncertainties, the fits to the diffusion model describe the experimental data very well (compare examples in figure 1 (c)). This seems to confirm that at least the overall trends and magnitudes of the parameters k_{chem} and D_{chem} are reliable.

Figure S-1 (supplementary material) shows a comparison of the present results obtained at 800°C with those from earlier studies on the long-term stability of the oxygen exchange kinetics of LSC at 600 [21, 22] and 700°C [13]. In dry atmospheres, either without or with a Cr and Si source, the initial values of k_{chem} and D_{chem} of the fresh samples remain stable for

1000-2000 h at 600-800°C with negligible or small degradation. All samples show a significant decrease in both kinetic parameters at 600-800°C when the atmospheres are humidified. The relative decrease in the values of the kinetic parameters, $k_{chem}(t)/k_{chem}(t=0)$ and $D_{chem}(t)/D_{chem}(t=0)$, is greatest at 700°C. At 600°C, the relative stability of the oxygen exchange properties is higher than at 700°C, even though the absolute values of k_{chem} and D_{chem} of the fresh samples are lower due to the thermally activated nature of both parameters. At 800°C the lowest relative decrease in k_{chem} and D_{chem} is found. A possible explanation of this behavior could be two counteracting effects: On the one hand, the gas phase concentrations of the volatile Cr and Si species $CrO_2(OH)_2$, CrO_3, and $Si(OH)_4$, which are responsible for the degradation, increase with increasing temperature as shown in figure 2 (for specific values see supplementary material). On the other hand, the thermodynamic stability of the perovskite phase LSC relative to the chromates and silicates should increases with increasing temperature. This is illustrated by phase diagram calculations of LSC vs. $pCrO_2(OH)_2$ in humid atmosphere (supplementary material). At pO_2=0.10 bar and 100 % relative humidity (pO_2=0.0316 atm), the decomposition of LSC is shifted to higher $pCrO_2(OH)_2$ with increasing temperature. Analogous phase equilibrium calculations for Si poisoning of LSC could not be performed due to lack of thermodynamic data. However, it could be assumed that the stability of LSC vs. Si poisoning shows a similar trend. Therefore, secondary phases (silicates) should also be more easily formed at lower temperatures.

3.2 Scanning electron microscopy

Figure 4 shows high resolution SEM images of the fresh and degraded LSC surfaces. The fresh sample (figure 4 (a)) exhibits a relatively smooth and dense surface (superficial grain pull-out is due to the polishing process). After 1300 h in dry atmosphere with exposure to Cr and Si few, small crystals appear at the surface (figure 4 (b); for additional image see

supplementary material). After additional 1100 h in the humidified test gas with 30 % relative humidity, a lot of irregularly shaped particles with several µm lengths are found next to thin needle-like crystals (figure 4 (c); additional images can be found in the supplementary material). After additional 1000 h in an atmosphere with 60 % relative humidity (figure 4 (d); additional images can be found in the supplementary material) the size of the crystals and the coverage of the surface have further increased. EDXS and WDXS elemental mapping (figure 5) after 3400 h of testing shows that the degraded surface is enriched with Sr and La, while the Co concentration is rather low. Evidence of Cr and Si contamination is also found on the surface (figure 5; additional images can be found in the supplementary material).

The Z-contrast in the BSE images of those samples which were exposed to Cr and Si sources in humidified atmospheres (for images see supplementary material) indicates that the crystallites have different chemical compositions. EDXS analyses of different points on the degraded surface were performed (see supplementary material). In addition to the original bulk phase LSC, large crystallites consisting of $SrCrO_4$ were found. The presence of this phase is also confirmed in the STEM results (section 3.4).

3.3 X-ray photoelectron spectroscopy

XPS elemental depth profiles of fresh and degraded LSC samples are given in figure 6. The fresh sample (figure 6 (a)) shows a homogeneous depth distribution of the elements La, Sr, and Co, with the exception of a Sr-enriched and La-depleted zone observed at the immediate surface. This is an effect which has been frequently found with freshly prepared and degraded samples as reported in the literature by various authors (for instance [5, 23-25]). No Cr or Si contaminations were observed in the fresh sample. After 1300 h in dry atmosphere with exposure to Cr and Si sources, the width of the Sr-enriched zone has increased, but still no Cr contamination is found (figure 6 (b)). This is in agreement with the thermodynamic data in

figure 2 which show that under dry conditions the predominating Cr-containing gas phase species, CrO_3, has a relatively low partial pressure (see also supplementary material). In comparison, those degraded samples which were exposed to Cr and Si sources in humidified atmospheres show a significant contamination with chromium (figures 6 (c) and (d)). The Cr and Sr signals show the same trends in the concentration vs. depth dependence. Approximately 900 nm of material had to be removed from the surface by Ar-sputtering until the Cr signal dropped below the detection limit and the Sr signal reached the concentration which was observed with the fresh sample. This is presumably due to the presence of the relatively large $SrCrO_4$ crystals on the degraded surface, as can also be seen in the SEM and STEM images (sections 3.2 and 3.4). In addition, the Co concentration at the surface of the samples in figures 6 (c) and (d) is much lower than with the specimens in figures 6 (a) and (b). After a certain time of Ar-sputtering (in a certain sample depth) a constant composition over depth is reached in the XPS elemental depth profiles in figure 6. However, it should be noted that this composition will usually deviate from the nominal (bulk) composition of LSC due to the effect of preferential sputtering [26].

Silicon could not be detected by XPS due to peak overlap with other elements. However, the Si-contamination of the near-surface region could be clearly shown by SEM-WDXS (figure 5; additional images see supplementary material) and STEM (figure 8).

3.4 Scanning transmission electron microscopy

Figure 7 shows STEM images of the degraded LSC sample after 3400 h of testing. Different gray scales in the high angle annular dark field (HAADF) imaging mode indicate that different phases are formed at the surface and at the grain boundaries in the near-surface region (compare also images in the supplementary material). The chemical composition of

these phases could be determined by STEM-EDXS and -EELS. The oxygen exchange-active bulk phase LSC is evident in figure 7 in the light gray regions (for instance: region 1, marked in the figure) in the interior of the large grains. The large dark gray grains in figure 7 which occur mainly at the immediate surface (for instance: region 2, marked in the figure) could be identified as $SrCrO_4$. Between these particles a La-silicate phase, which contains also some Sr was found in the medium gray regions in figure 7 (for instance: region 3, marked in the figure). Figure 8 gives STEM-EDXS and -EELS elemental maps of the strongly degraded surface region. Coexisting phases of $SrCrO_4$ and La-(Sr-)silicate are identified on top of the LSC bulk phase. Besides, some Co_3O_4 grains were found at the surface and at grain boundaries (figure 8; additional images can be found in the supplementary material) which result from the phase decomposition of LSC due to impurity poisoning. The formation of $SrCrO_4$ and Co_3O_4 particles was also observed in an earlier study on Cr poisoning of LSC64 at 700°C [12], as well as by other authors on Cr-poisoned $La_{0.6}Sr_{0.4}Co_{0.2}Fe_{0.8}O_{3-\delta}$ samples at 800°C [5].

4. Summary

The long-term stability of the oxygen exchange kinetics of the intermediate temperature solid oxide fuel cell cathode material $La_{0.6}Sr_{0.4}CoO_{3-\delta}$ (LSC) was investigated. In-situ dc-conductivity relaxation measurements were performed for 3400 h at 800°C in dry and humidified atmospheres in the absence and presence of chromium and silicon sources. Under dry conditions high values of the chemical surface exchange coefficient k_{chem} and the chemical bulk diffusion coefficient of oxygen D_{chem} were found. The kinetic parameters remained stable during 1300 h in dry atmosphere without or with the presence of Cr and Si sources. However, when the test gas was humidified (30-60 % relative humidity), a

significant decrease in k_{chem} and D_{chem} was observed. Post-test analyses of degraded samples showed that secondary phases were formed on the surface and at the grain boundaries of the degraded LSC sample. In the near-surface region large $SrCrO_4$ and La-(Sr-)silicate crystals were found. In addition, smaller grains of Co_3O_4 formed at the surface and at the grain boundaries. Therefore, the observed decrease in the oxygen exchange kinetics, which occurs especially in humid atmospheres in the presence of Cr and Si sources, could be ascribed to the phase decomposition of the active bulk phase LSC into inactive secondary phases. It is concluded that the use of dry air in technical SOFC applications could significantly reduce the degradation of LSC and similar La- and Sr-containing cathode materials.

Acknowledgment

Financial support provided by the Austrian 'Klima- und Energiefonds' and AVL List GmbH (Austria) within the program 'Neue Energien 2020' (project no. 834431, project title ELTSECCS) is gratefully acknowledged. F. Hofer thanks for partial funding from the European Union within the 7th Framework Programme (FP7/2007-2013) under Grant Agreement No.312483 (ESTEEM2). Furthermore, the authors would like to thank S. Šimić and M. Dienstleder (Graz Center for Electron Microscopy) for SEM-EDXS/-WDXS measurements and the FIB preparation, as well as G. Hawranek (Montanuniversitaet Leoben) for additional SEM analyses.

References

[1] K. Kendall, M. Kendall, Editors, *High-temperature Solid Oxide Fuel Cells for the 21st Century*, Academic Press, Oxford, UK (2016).

[2] K.-D. Kreuer, Editor, *Fuel Cells - Selected Entries from the Encyclopedia of Sustainability Science and Technology*, Springer-Verlag, New York (2013).

[3] S.C. Singhal, K. Kendall, *High temperature solid oxide fuel cells: fundamentals, design and applications*, Elsevier Advanced Technology, The Boulevard, Langford lane, Kidlington, Oxford OX5, UK (2004).

[4] M. Stanislowski, E. Wessel, K. Hilpert, T. Markus, L. Singheiser, *J. Electrochem. Soc.* **154** (4) (2007) A295.

[5] L. Zhao, J. Drennan, C. Kong, S. Amarasinghe, S.P. Jiang, *Journal of Materials Chemistry A* **2** (29) (2014) 11114.

[6] E. Konysheva, H. Penkalla, E. Wessel, J. Mertens, U. Seeling, L. Singheiser, K. Hilpert, *J. Electrochem. Soc.* **153** (4) (2006) A765.

[7] R. Trebbels, T. Markus, L. Singheiser, *J. Fuel Cell Sci. Technol.* **7** (1) (2009) 011013/1.

[8] T. Horita, H. Kishimoto, K. Yamaji, M.E. Brito, Y. Xiong, H. Yokokawa, Y. Hori, I. Miyachi, *J. Power Sources* **193** (1) (2009) 194.

[9] P. J. Howard, I. Szkoda, *J. Fuel Cell Sci. Technol.* **9** (4) (2012) 041009/1.

[10] J.A. Schuler, Z. Wuillemin, A. Hessler-Wyser, J. Van herle, *Electrochem. Solid-State Lett.* **14** (2) (2011) B20.

[11] A. Egger, E. Bucher, M. Yang, W. Sitte, *Solid State Ionics* **225** (2012) 55.

[12] N. Schrödl, E. Bucher, C. Gspan, A. Egger, C. Ganser, C. Teichert, F. Hofer, W. Sitte, *Solid State Ionics* **288** (2016) 14.

[13] N. Schrödl, E. Bucher, A. Egger, P. Kreiml, C. Teichert, T. Höschen, W. Sitte, *Solid State Ionics* **276** (2015) 62.

[14] E. Bucher, W. Sitte, F. Klauser, E. Bertel, *Solid State Ionics* **208** (2012) 43.

[15] J.A. Lane, J.A. Kilner, *Solid State Ionics* **136-137** (2000) 997.

[16] W. Preis, E. Bucher, W. Sitte, *Solid State Ionics* **175** (2004) 393.

[17] W. Preis, E. Bucher, W. Sitte, *J. Power Sources* **106** (2002) 116.

[18] W. Preis, M. Holzinger, W. Sitte, *Monatsh. Chem.* **132** (2001) 499.

[19] J. Crank, *The mathematics of diffusion*, Oxford University Press, Oxford, UK (2011).

[20] R. Behrisch, W. Eckstein, *Sputtering by Particle Bombardment, Topics in Applied Physics, Vol. 110*, Springer, Berlin Heidelberg (2007).

[21] E. Bucher, M. Yang, W. Sitte, *J. Electrochem. Soc.* **159** (5) (2012) B592.

[22] E. Bucher, M. Yang, W. Sitte, In-situ investigation of the chromium induced degradation of the oxygen exchange kinetics of the IT-SOFC cathode material $La_{0.6}Sr_{0.4}CoO_{3-\delta}$, In: S.C. Singhal, K. Eguchi, Editors, *12th Intern. Symp. Solid Oxide Fuel Cells (SOFC-XII)*, The Electrochemical Society, Pennington, USA, Montréal, Canada (2011), p.2019-2025.

[23] G.M. Rupp, H. Téllez, J. Druce, A. Limbeck, T. Ishihara, J. Kilner, J. Fleig, *Journal of Materials Chemistry A* **3** (45) (2015) 22759.

[24] Z. Cai, M. Kubicek, J. Fleig, B. Yildiz, *Chem. Mater.* **24** (6) (2012) 1116.

[25] P.A.W. van der Heide, *Surf. Interface Anal.* **33** (5) (2002) 414.

[26] D. Tonti, R. Zanoni, Measurement methods - Electronic and chemical properties: X-Ray photoelectron spectroscopy, in: J. Garche, Editor, *Encyclopedia of electrochemical power sources*, Elsevier, Amsterdam (2009), p.673-695.

[27] E.J. Opila, N.S. Jacobson, D.L. Myers, E.H. Copland, *JOM* **58** (1) (2006) 22.

[28] N.S. Jacobson, E.J. Opila, D.L. Myers, E.H. Copland, *J. Chem. Thermodyn.* **37** (10) (2005) 1130.

[29] K. Huang, J.B. Goodenough, *Solid oxide fuel cell technology - Principles, performance and operations*, Woodhead Publishing Limited, Cambridge, UK (2009).

[30] E.J. Opila, D.L. Myers, N.S. Jacobson, I.M.B. Nielsen, D.F. Johnson, J.K. Olminsky, M.D. Allendorf, *J. Phys. Chem. A* **111** (10) (2007) 1971.

Figure Captions

Fig. 1 (a) Chemical surface exchange coefficient (k_{chem}) and (b) chemical diffusion coefficient of oxygen (D_{chem}) of LSC at 800°C and $1.0\times10^{-1} \leq pO_2/bar \leq 1.5\times10^{-1}$ as a function of time; Test intervals in dry and humidified atmospheres without (wo) and with (w) Cr and Si sources are indicated by vertical lines and corresponding labels. (c) Examples for electrical conductivity relaxation curves at different stages of the long-term stability test; (1) fresh sample, (2) dry atmosphere with Si source and without Cr source, (3) 30 % relative humidity with Si and Cr source, (4) 60 % relative humidity with Si and Cr source. Fits of the diffusion model are shown as dashed lines.

Fig. 2 Partial pressures of $CrO_2(OH)_2(g)$, $CrO_3(g)$, and $Si(OH)_4(g)$ at pO_2=0.10 bar as a function of temperature and water content of the gas phase; Estimations of $pSi(OH)_4$ are based on thermodynamic data from [27, 28]. Estimations of $p(CrO_2(OH)_2)$ and $pCrO_3$ were made with data from [27, 29, 30].

Fig. 3 Electrical conductivity of LSC at 800°C as a function of time at different oxygen partial pressures; Test intervals in dry and humidified atmospheres without (wo) and with (w) Cr and Si sources are indicated by vertical lines and corresponding labels.

Fig. 4 SEM-SE images of LSC surfaces (a) in the fresh state, (b) after 1300 h in dry atmosphere, (c) after additional 1100 h in atmosphere with 30 % relative humidity, (d) after additional 1000 h in atmosphere with 60 % relative humidity; samples (b)-(d) were exposed to Cr and Si.

Fig. 5 SEM-SE image and EDXS/WDXS elemental maps of the degraded LSC surface after 3400 h of testing; the sample was exposed to Cr and Si. The width of all images is 108.8 µm.

Fig. 6 XPS elemental depth profiles of LSC surfaces (a) in the fresh state, (b) after 1300 h in dry atmosphere, (c) after additional 1100 h in atmosphere with 30 % relative humidity, (d) after additional 1000 h in atmosphere with 60 % relative humidity; samples (b)-(d) were exposed to Cr and Si.

Fig. 7 STEM HAADF cross-sectional images from the near-surface region of LSC after 3400 h of testing; the sample was exposed to Cr and Si; characteristic regions (1, 2, and 3) marked in the image are discussed in the text.

Fig. 8 STEM cross-sectional image and EDXS/EELS elemental mappings from the near-surface region of LSC after 3400 h of testing; RGB images show the distribution of different phases. The sample was exposed to Cr and Si.

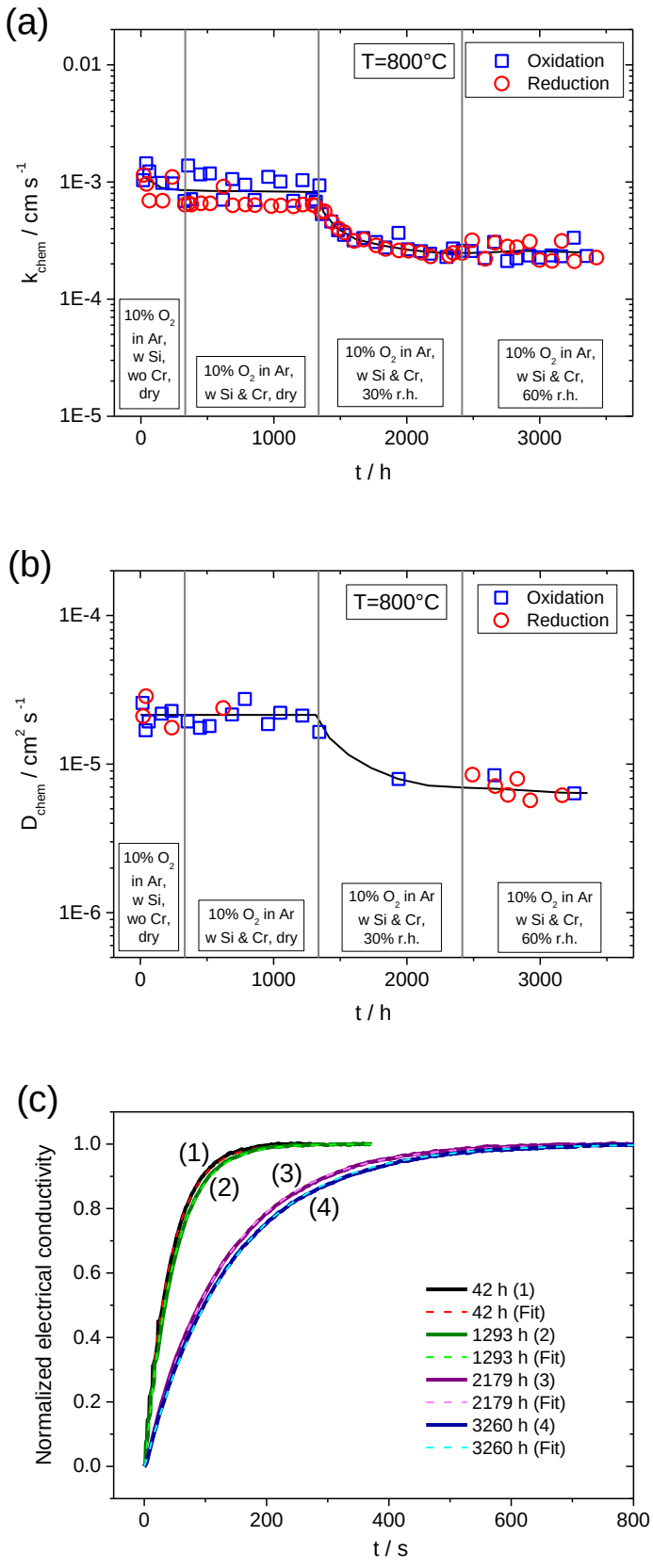
(a)
T=800°C
Oxidation
Reduction
0.01
1E-3
1E-4
1E-5
k_chem / cm s^-1
10% O2 in Ar, w Si, wo Cr, dry
10% O2 in Ar, w Si & Cr, dry
10% O2 in Ar, w Si & Cr, 30% r.h.
10% O2 in Ar, w Si & Cr, 60% r.h.
0
1000
2000
3000
t / h
(b)
T=800°C
Oxidation
Reduction
1E-4
1E-5
1E-6
D_chem / cm^2 s^-1
10% O2 in Ar, w Si, wo Cr, dry
10% O2 in Ar w Si & Cr, dry
10% O2 in Ar w Si & Cr, 30% r.h.
10% O2 in Ar w Si & Cr, 60% r.h.
0
1000
2000
3000
t / h
(c)
Normalized electrical conductivity
1.0
0.8
0.6
0.4
0.2
0.0
(1)
(2)
(3)
(4)
42 h (1)
42 h (Fit)
1293 h (2)
1293 h (Fit)
2179 h (3)
2179 h (Fit)
3260 h (4)
3260 h (Fit)
0
200
400
600
800
t / s

Figure 1.

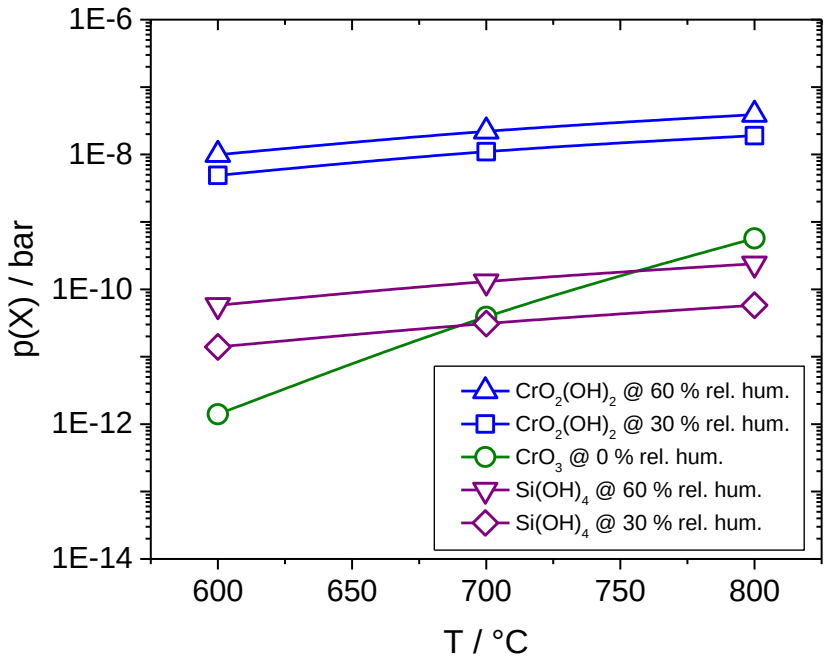
1E-6
1E-8
1E-10
1E-12
1E-14
p(X) / bar
600
650
700
750
800
T / °C
CrO2(OH)2 @ 60 % rel. hum.
CrO2(OH)2 @ 30 % rel. hum.
CrO3 @ 0 % rel. hum.
Si(OH)4 @ 60 % rel. hum.
Si(OH)4 @ 30 % rel. hum.

Figure 2.

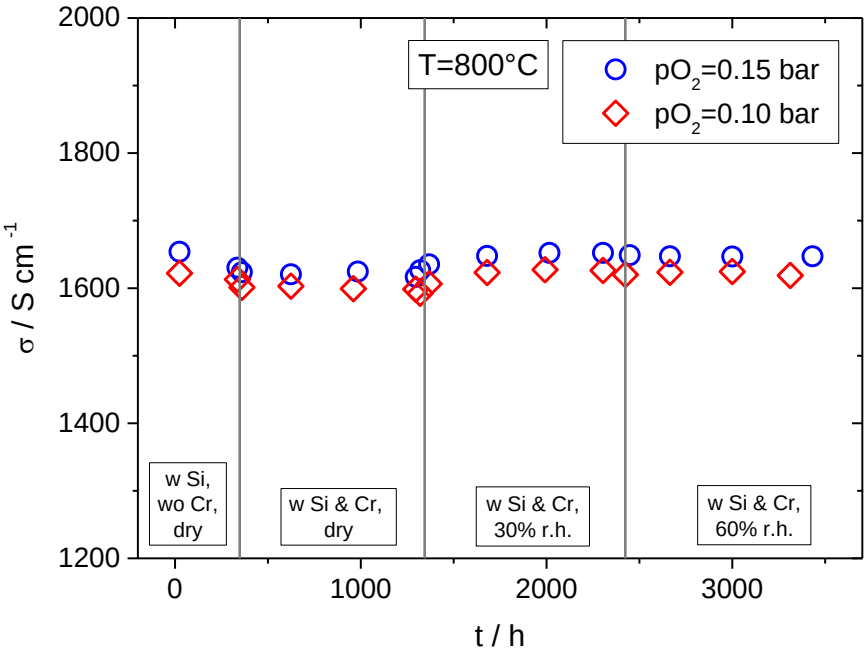
T=800°C
pO2=0.15 bar
pO2=0.10 bar
w Si, wo Cr, dry
w Si & Cr, dry
w Si & Cr, 30% r.h.
w Si & Cr, 60% r.h.
σ / S cm-1
t / h
2000
1800
1600
1400
1200
0
1000
2000
3000

Figure 3.

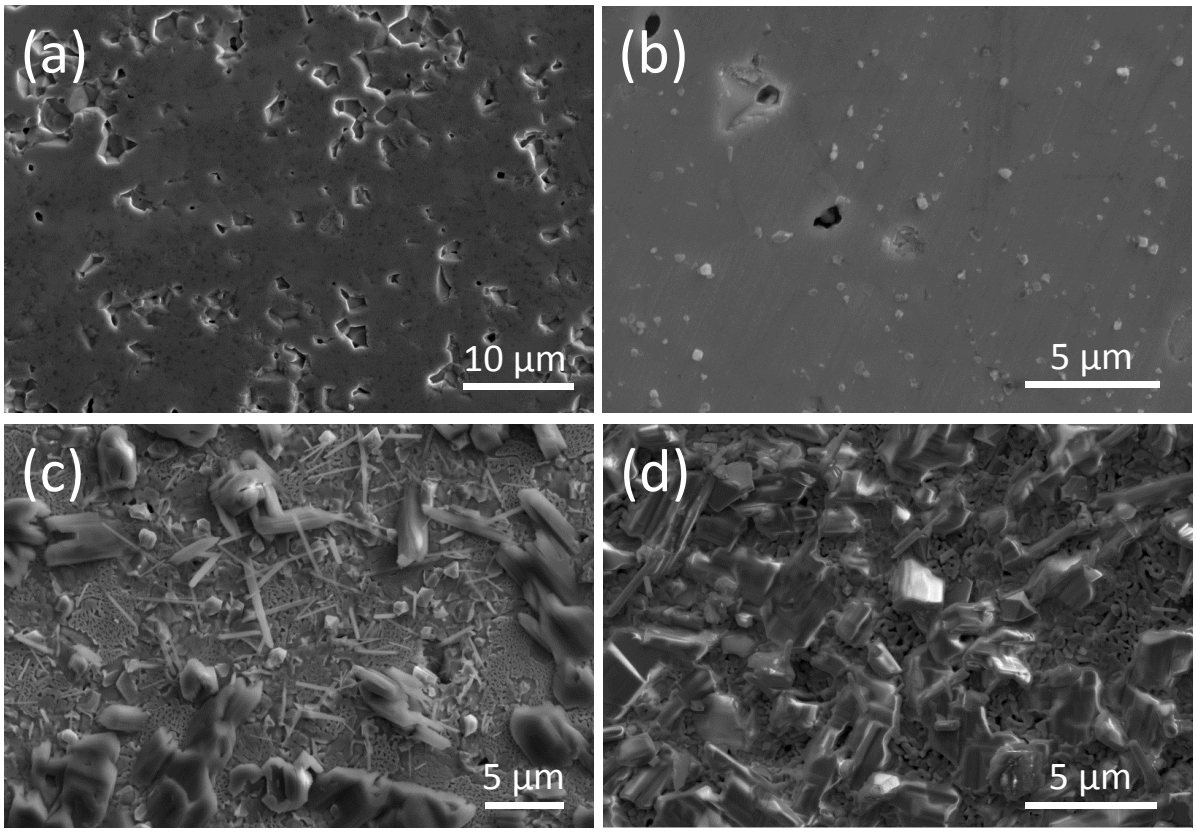

Figure 4.

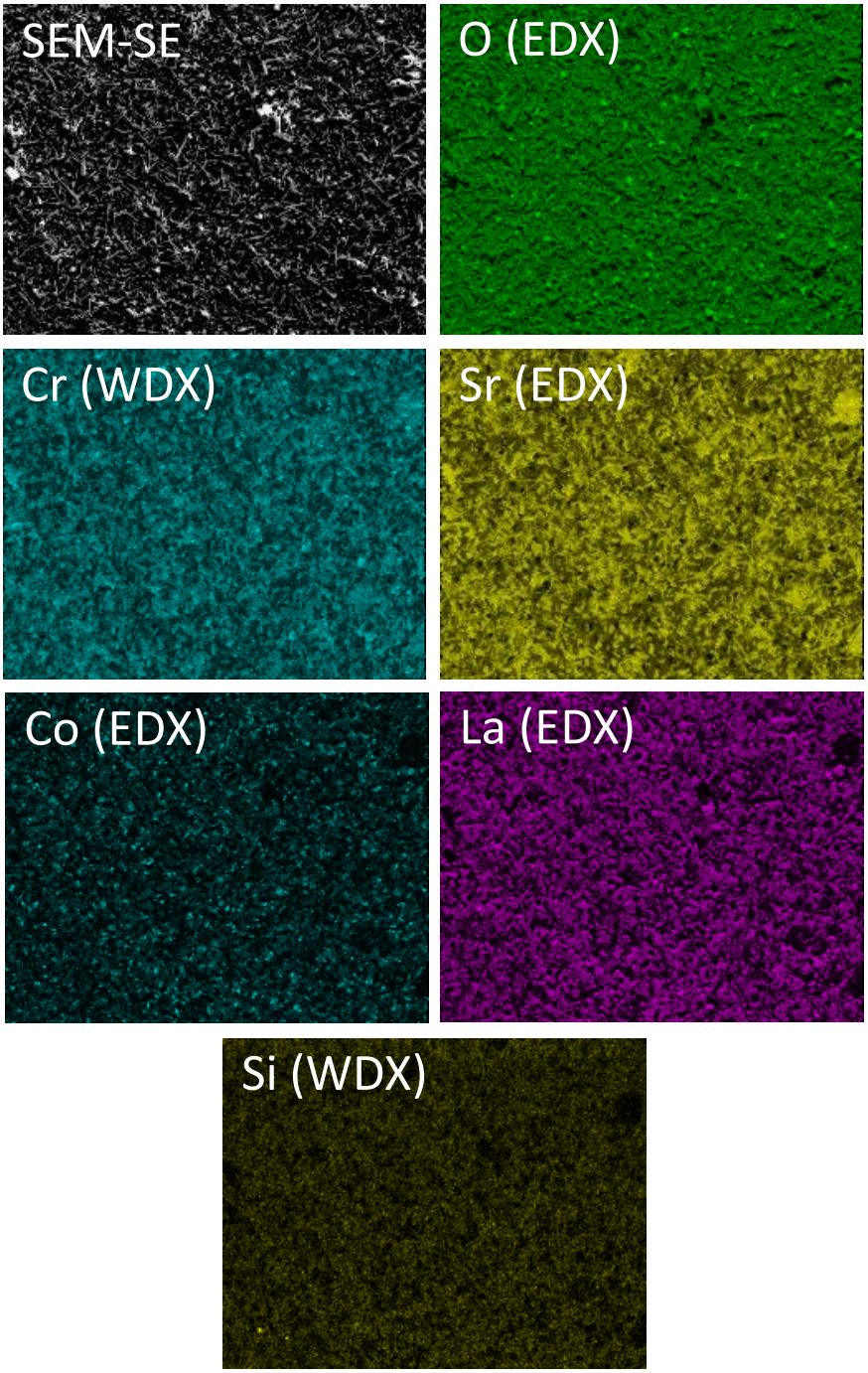

Figure 5.

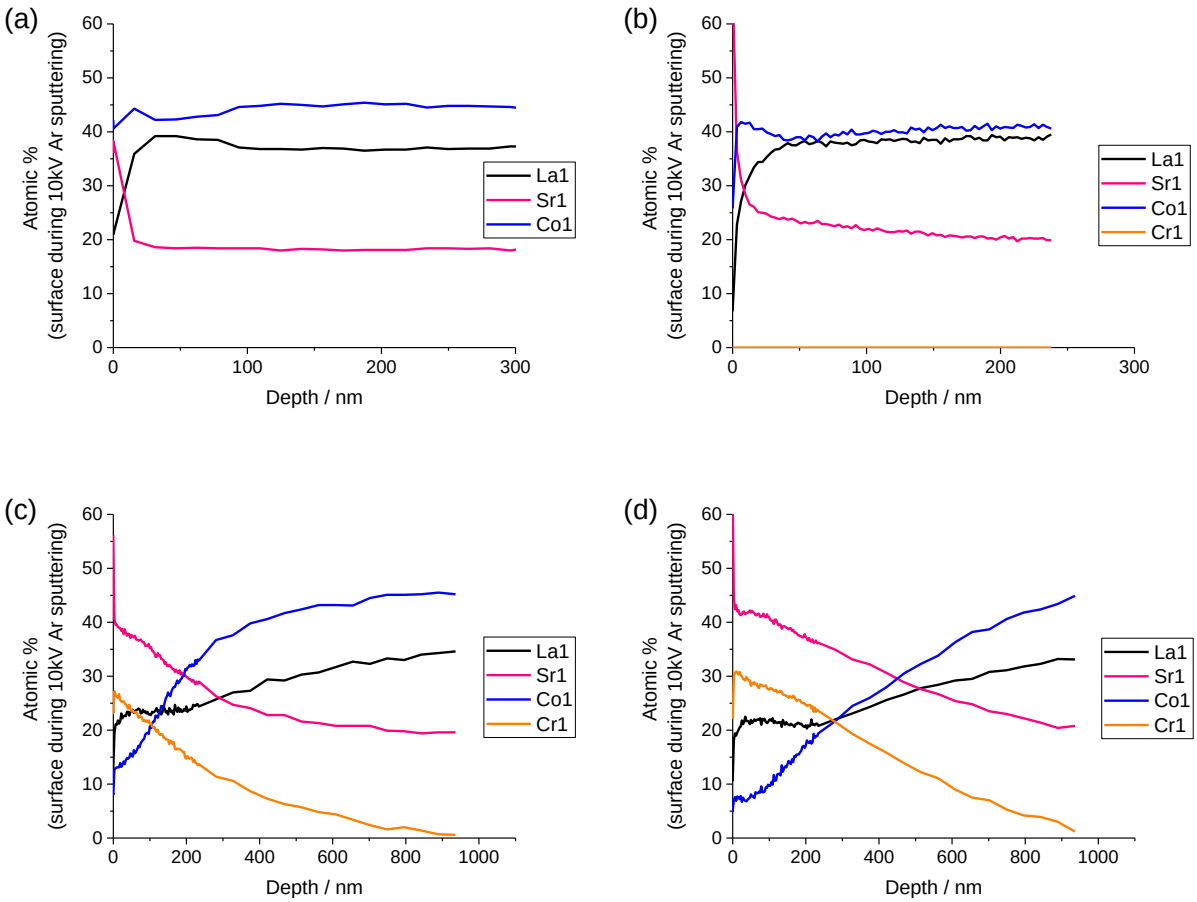
(a)
(b)
(c)
(d)
Atomic %
(surface during 10kV Ar sputtering)
Depth / nm
La1
Sr1
Co1
Cr1

Figure 6.

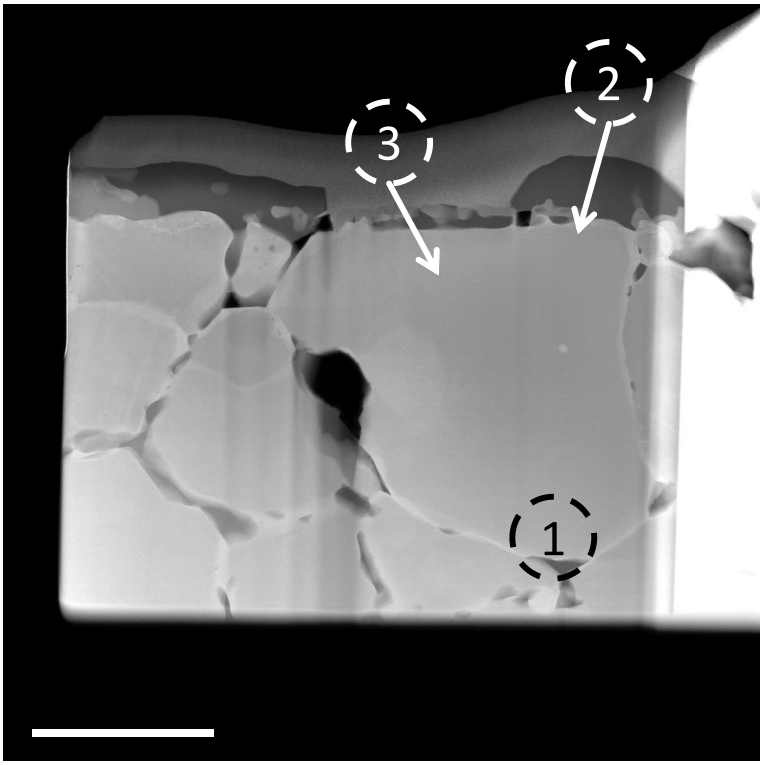

Figure 7.

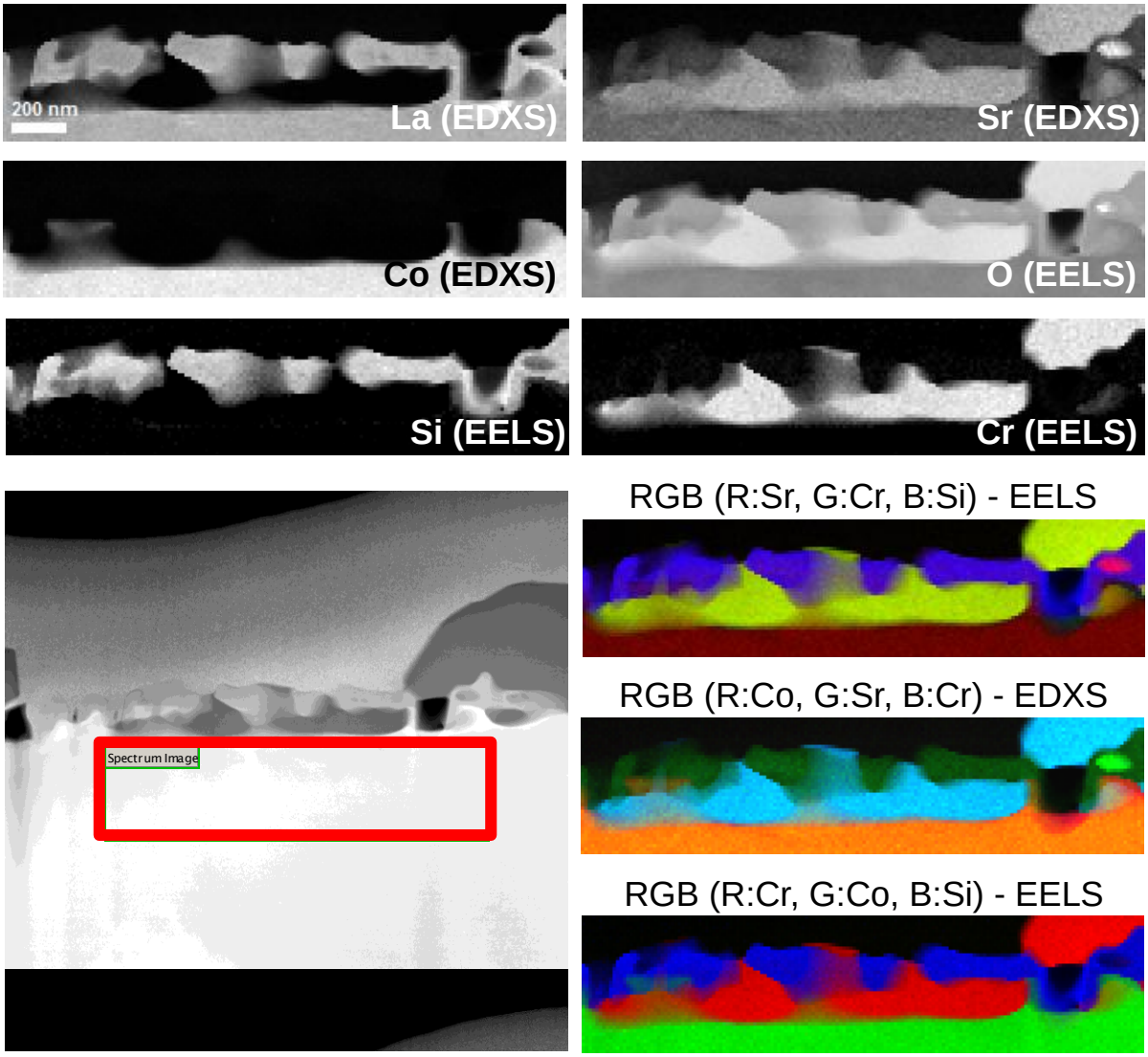
200 nm
La (EDXS)
Sr (EDXS)
Co (EDXS)
O (EELS)
Si (EELS)
Cr (EELS)
RGB (R:Sr, G:Cr, B:Si) - EELS
Spectrum Image
RGB (R:Co, G:Sr, B:Cr) - EDXS
RGB (R:Cr, G:Co, B:Si) - EELS

Figure 8.